Materials Advances

ROYAL SOCIETY OF CHEMISTRY

PAPER

View Article Online
View Journal | View Issue

Cite this: *Mater. Adv.*, 2026, 7, 3247

Suppression of the metal-to-semiconductor transition in nanocrystalline Ti_4O_7 *via* crystallite size control

Tomoko Kubota, [a] Riku Seiki, [a] Takahiro Kondo, [ab] Verdad C. Agulto, [c] Makoto Nakajima, [c] Shin-ichi Ohkoshi [d] and Hiroko Tokoro *[ad]

Received 13th December 2025,
Accepted 21st January 2026

DOI: 10.1039/d5ma01459j

rsc.li/materials-advances

Nanocrystalline Ti_4O_7 with controlled crystallite sizes was synthesized to investigate the effect of crystallite size on the metal–semiconductor transition. Magnetic susceptibility measurements revealed that the transition fraction for Ti_4O_7 with an average crystallite size of 11 nm was approximately 60% of that observed for Ti_4O_7 with a crystallite size of 30 nm, indicating suppression of the phase transition. Differential scanning calorimetry (DSC) showed that the observed transition enthalpies were 302 J mol^{-1} and 850 J mol^{-1} for the smaller and larger crystallite sizes, respectively, showing a reduction in the transition enthalpy with decreasing crystallite size. Thermodynamic calculations suggest that this suppression arises from surface energy contributions, which reduce the transition enthalpy with decreasing crystallite size. These results indicate that reducing the crystallite size offers an effective means of controlling the metal–semiconductor transition in Ti_4O_7, contributing to the development of tunable phase-transition materials for advanced functional materials.

Introduction

Magnéli phase titanium oxides, with the general formula Ti_nO_{2n-1} ($3 \leq n \leq 9$), represent a fascinating class of materials known for their diverse functional properties, including electrical conductivity,[1–7] electrochemical performance,[8–24] heat storage capability,[25–36] and switching behavior.[37–42] Among these, Ti_4O_7 is particularly noteworthy, as it exhibits metallic behavior at room temperature and possesses the highest electrical conductivity of any known metal oxide. Owing to these exceptional properties, Ti_4O_7 has attracted significant attention for potential applications in fuel cells and electrode catalysts, prompting extensive research in these areas.[8–10,12,14,17–22] The single crystal of Ti_4O_7 undergoes a two-step phase transition involving metallic, disordered, and ordered semiconductor phases as a function of temperature.[1,2,43–47] At room temperature, Ti_4O_7 exists in a high-temperature (HT) metallic phase. Upon cooling to 150 K, it undergoes a transition to an intermediate-temperature (IT) semiconductor phase, followed by a further transition at 130 K to a low-temperature (LT) ordered semiconductor phase (Fig. 1). In the HT phase, all the Ti atoms adopt a $Ti^{3.5+}$ state in a charge-delocalized system. In contrast, the IT phase is a charge-localized state comprising distinct Ti^{3+} and Ti^{4+} ions. The transition from the IT to the LT phase corresponds to an order–disorder transition, where the randomly distributed Ti^{3+} and Ti^{4+} ions become arranged in an ordered configuration. These transitions are designated phase transition **I** (HT → IT) and phase transition **II** (IT → LT), respectively. Theoretical studies have predicted the emergence of superconductivity in Ti_4O_7,[48–50] spurring efforts to realize superconductivity by applying pressure to the semiconductor LT phase or by stabilizing the metallic HT phase at room temperature.[51,52] Since the 1970s, extensive efforts have been made to control the phase transitions in Ti_4O_7 *via* vanadium substitution.[43,53–56] Although these studies did not succeed in stabilizing the HT metallic phase at low temperatures, they did report the suppression of phase transition **II**. More recently, in 2017, introducing oxygen vacancies into Ti_4O_7 thin films was reported to suppress phase transition **I** and **II**, thereby retaining the metallic phase at low temperatures and inducing superconductivity.[57] In 2020, we demonstrated that reducing the crystallite size of Ti_4O_7 to approximately 50 nm suppresses phase transition **II**, resulting in a simplified, one-step phase transition *via* phase transition **I** only.[58]

[a] *Department of Materials Science, Institute of Pure and Applied Sciences University of Tsukuba 1-1-1 Tennodai, Tsukuba, Ibaraki 305-8573, Japan. E-mail: tokoro.hiroko.gp@u.tsukuba.ac.jp*
[b] *Tsukuba Institute for Advanced Research (TIAR) University of Tsukuba 1-1-1 Tennodai, Tsukuba, Ibaraki 305-8577, Japan*
[c] *Institute of Laser Engineering The University of Osaka 2-6 Yamadaoka, Suita, Osaka, 565-0871, Japan*
[d] *Department of Chemistry, School of Science The University of Tokyo 7-3-1 Hongo, Bunkyo-ku, Tokyo, 113-0033, Japan*

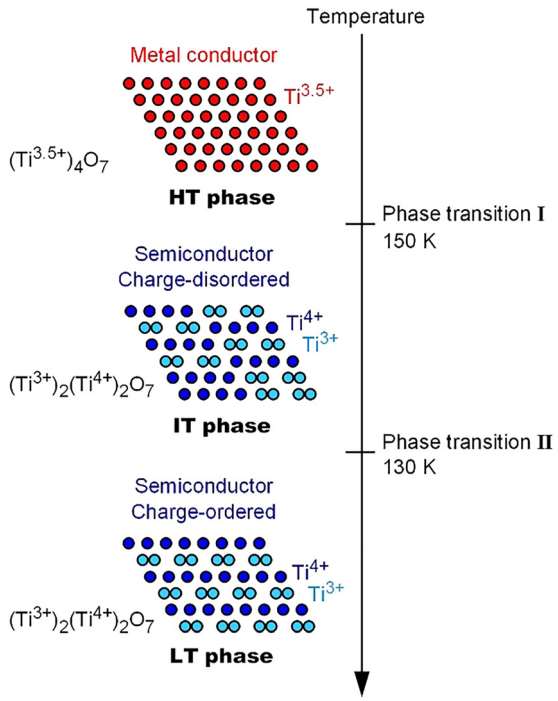

Fig. 1 Schematic illustration of the two-step phase transition in a single crystal of Ti_4O_7. The high-temperature (HT) metallic phase transforms into an intermediate-temperature (IT) semiconductor at approximately 150 K (phase transition **I**), followed by a second transition to a low-temperature (LT) semiconductor phase near 130 K (phase transition **II**). In the HT phase, Ti ions exhibit a mixed valence state of $Ti^{3.5+}$, and separate into Ti^{3+} and Ti^{4+} ions in the IT and LT phases.

In this study, we investigated the effect of crystallite size on phase transition **I** by synthesizing Ti_4O_7 nanocrystals with further reduced dimensions. Starting from titanium chloride, a precursor was synthesized and subsequently subjected to annealing *via* hydrogen reduction to obtain Ti_4O_7 samples with average crystallite sizes of 11 and 30 nm. Temperature-dependent measurements revealed that smaller crystallite sizes led to a more pronounced suppression of the phase transition. Thermodynamic modelling using a mean-field approximation suggested that this suppression arises from the contribution of surface energy to the Gibbs free energy.

Results and discussion

Materials and characterization

A mixed solution containing 420 mL of H_2O, 1.40 mL of $TiCl_4$, and 9.60 mL of aqueous NH_3 (25 wt%) was prepared in a 1-L container. The solution was stirred at 50 °C for 20 h in an oil bath, forming $Ti(OH)_4$ precipitates (eqn (1)).[35] These precipitates were separated by centrifugation, washed with ethanol, and dried at 60 °C for 24 h,

$$TiCl_4 + 4H_2O + 4NH_3 \rightarrow Ti(OH)_4 + 4NH_4Cl. \quad (1)$$

The resulting precipitate was then calcined under hydrogen flow for 5 h under two different conditions: 1.0 dm3 min^{-1} at 950 °C for **1** and 0.5 dm^3 min^{-1} at 1000 °C for **2**, forming a black powder,

$$4Ti(OH)_4 + H_2 \rightarrow Ti_4O_7 + 9H_2O. \quad (2)$$

X-ray fluorescence (XRF) analysis confirmed the composition of the resulting powders to be $Ti_{4.00(8)}O_{7.00(8)}$; Calc.: Ti, 63.1 wt%. Found: Ti, 63.1(8) wt% for **1**, and $Ti_{4.00(8)}O_{7.00(8)}$; Calc.: Ti, 63.1 wt%. Found: Ti, 63.0(6) wt% for **2**.

Crystallite size and morphology

Room-temperature X-ray powder diffraction (XRD) patterns and Rietveld analysis confirmed that the synthesized samples of **1** and **2** were pure Ti_4O_7 with a triclinic crystal structure (space group: $P\bar{1}$ (Fig. 2a and b). The refined lattice parameters were as follows: **1**: a = 5.5980(5) Å, b = 7.1294(5) Å, c = 12.4514(10) Å, α = 95.070(6)°, β = 95.068(5)°, γ = 108.837(4)°, V = 464.87(6) Å^3, and for **2**: a = 5.5983(2) Å, b = 7.1241(2) Å, c = 12.4606(3) Å, α = 95.057(2) °, β = 95.147(2) °, γ = 108.777(2)°, V = 465.00(2) Å^3 (Tables S1–S4). These lattice parameters were consistent with those reported for Ti_4O_7.[45,47,58,59] The crystallite sizes, estimated by Rietveld analyses, were 11.1 ± 0.2 nm for **1** and 29.6 ± 0.4 nm for **2**. Scanning electron microscopy (SEM) images revealed that

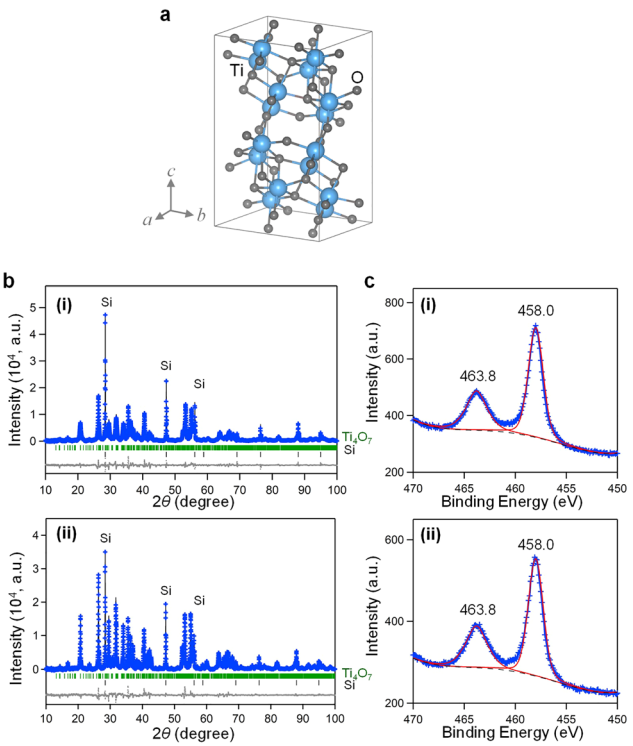

Fig. 2 Crystal structure and valence state of nanocrystalline Ti_4O_7. (a) Schematic representation of the crystal structure of Ti_4O_7. (b) XRD pattern and Rietveld analysis for (i) **1** and (ii) **2**. Blue circles indicate the observed data, black lines represent the calculated patterns, grey lines show the difference between observed and calculated data, and vertical bars mark the expected Bragg reflection positions for Ti_4O_7 (green) and the Si internal standard (grey). (c) XPS spectra of the Ti 2p peak for (i) **1** and (ii) **2**. Blue markers indicate the observed data, red lines represent the fitted peaks using a Voigt function, and black dashed lines show the background.

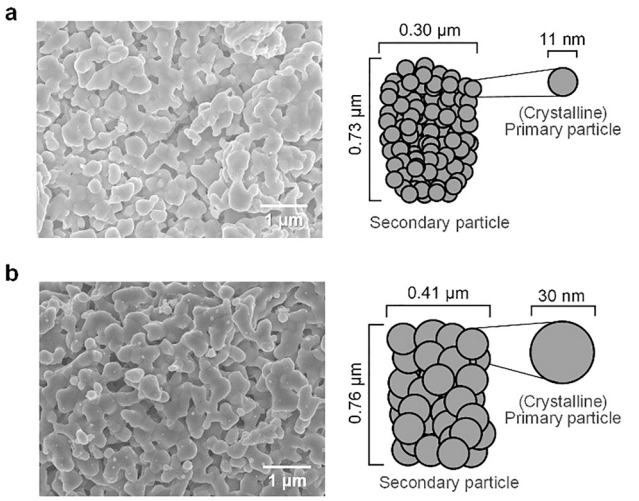

Fig. 3 SEM image (left) and schematic representation of particle morphology (right) for (a) **1** and (b) **2**.

both samples exhibited coral-like morphologies with dimensions of 0.73 ± 0.30 μm in the major axis and 0.30 ± 0.12 μm in the minor axis for **1**, and 0.76 ± 0.24 μm in the major axis and 0.41 ± 0.15 μm in the minor axis for **2** (Fig. 3 and Fig. S1). Transmission electron microscopy (TEM) confirmed that both samples consisted of sintered crystallites several tens of nanometers in size and that the crystallites of **2** were larger than those of **1** (Fig. S2). Combining XRD, Rietveld analysis, and SEM imaging, **1** was found to consist of secondary particles with a size of approximately 0.7 μm in the major axis and 0.3 μm in the minor axis, composed of primary crystallites of approximately 11 nm (Fig. 3a). In contrast, **2** comprised secondary particles with a size of approximately 0.8 μm in the major axis and 0.4 μm in the minor axis, built from primary crystallites of approximately 30 nm. X-ray photoelectron spectroscopy (XPS) profiles recorded at room temperature are shown in Fig. 2c and Fig. S3, and S4. The observed binding energy peaks at 458.0 eV (Fig. 2c), 463.8 eV (Fig. 2c), and 529.4 eV (Fig. S3 and S4) correspond to Ti $2p_{3/2}$, Ti $2p_{1/2}$, and O 1s, respectively. These values are consistent with those reported for the HT phase of bulk Ti_4O_7,[29,60] indicating that the Ti centers in the synthesized Ti_4O_7 (**1** and **2**) exhibit a valence state of +3.5 at room temperature, characteristic of the metallic phase (Fig. S5).

Temperature dependence of the magnetic susceptibility

The temperature dependence of magnetic susceptibility (χ_M) curves for **1** and **2** are shown in Fig. 4a and b, respectively. For both samples, χ_M decreases upon cooling, indicating a transition attributed to phase transition **I**, where the HT phase ($Ti^{3.5+}$) transforms into the IT phase comprising Ti^{3+} and Ti^{4+}. Defining the transition temperature as the temperature at which 50% of the transition occurs, the transitions for **1** were observed at 138 K (cooling) and 140 K (heating), whereas for **2**, these were observed at slightly higher temperatures at 146 K (cooling) and 147 K (heating). The transition amplitude in **1** was approximately 60% of that observed in **2**.

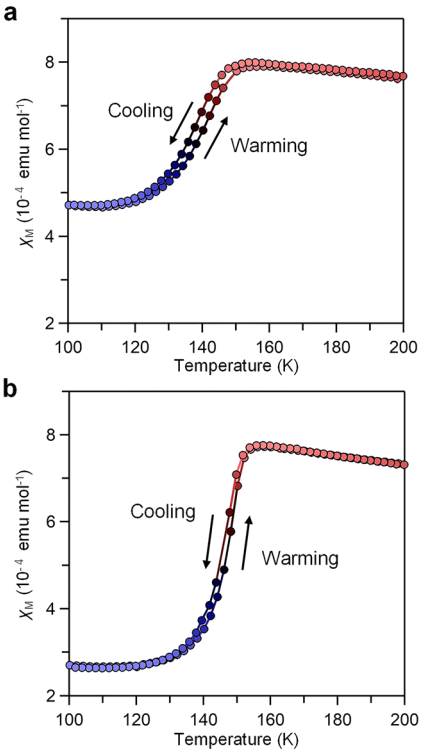

Fig. 4 χ_M *versus* temperature plot per mole of Ti_4O_7 for (a) **1** and (b) **2**, measured under an external magnetic field of 5000 Oe with a temperature sweep rate of ± 1.0 K min^{-1}.

Calorimetric measurement of the phase transition

To investigate the phase transition observed in the temperature dependence of the magnetic susceptibility, DSC measurements were performed to quantify the enthalpy change (Fig. 5). An endothermic peak was observed at 144 K for **1** and at 149 K for **2**. These peak positions aligned with the transition temperatures derived from magnetic susceptibility, confirming that **2** transitions occur at higher temperatures than for **1**. The observed transition enthalpies (ΔH_{obs}) were 302 ± 16 J mol^{-1}

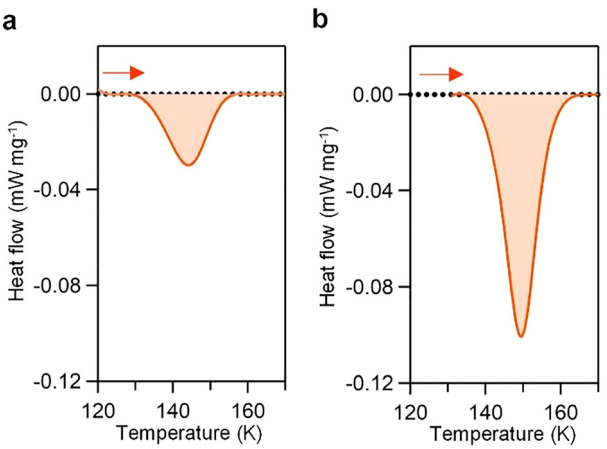

Fig. 5 DSC curves during the heating process for (a) **1** and (b) **2**, recorded at a temperature sweep rate of ± 20 K min^{-1}.

for **1** and 850 ± 33 J mol^{-1} for **2**, corresponding to approximately 15% and 43% of the values reported for bulk single crystals.[6] These results suggest that the transition enthalpy decreases with decreasing crystallite size.

Thermodynamic calculation for nano-crystalline Ti_4O_7

In this study, phase transition **II** was suppressed, and only phase transition **I** was observed. The transition fraction for **1** was approximately 60% of that for **2**, and the transition temperature was slightly lower for **1**. To understand this behavior, the Slichter-Drickamer (SD) model, a mean-field approximation equation that thermodynamically describes phase transitions,[61] was employed. In the SD model, the Gibbs free energy (G) is defined using the following equation: $G = x\,\Delta H_{trans} + \gamma\,x(1-x) + T\{R[x\ln x + (1-x)\ln(1-x)] - x\,\Delta S_{trans}\}$. Here, ΔH_{trans} and ΔS_{trans} are the transition enthalpy and entropy, respectively, and x represents the fraction of Ti_4O_7 units in the metallic phase, whereas $(1-x)$ corresponds to the semiconductor phase fraction. γ is the interaction parameter between the metallic and semiconductor phase units, and R is the gas constant. Based on the experimentally observed ΔH_{obs} and ΔS_{obs} values from DSC measurements for **1** and **2**, the calculated Gibbs free energy curves at various temperatures are shown in Fig. 6a and Fig. 6b, respectively. These curves showed that at high temperatures, the metallic phase is thermodynamically more stable (SI, S6). However, as the temperature decreases, a shift occurs, and below approximately 130 K, the semiconductor phase becomes more stable. The calculated transition temperatures were 146 K for **1** and 148 K for **2**. Although slight, this difference is consistent with magnetic susceptibility measurements, which similarly showed a slightly higher transition temperature of **2**.

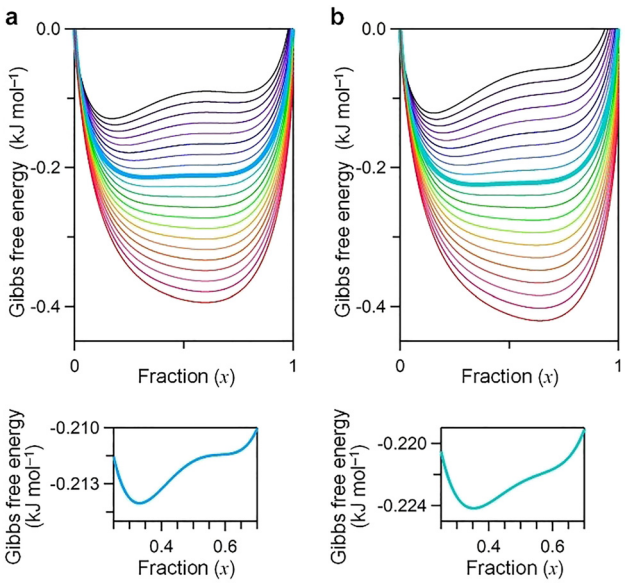

Fig. 6 Temperature-dependent Gibbs free energy (G) *versus* metallic-phase fraction (x) curves between the charge-delocalized and charge-localized phases for (a) **1** and (b) **2**, calculated using the Slichter-Drickamer mean-field model at 2 K intervals from 170 K to 130 K (upper panels). Enlarged views around the phase transition region are shown in the lower panel. The curve for **1** corresponds to 146 K, and that for **2** to 148 K. The thermodynamic parameters used were: ΔH_{trans} = 500 J mol^{-1}, ΔS_{trans} = 3.36 J K^{-1} mol^{-1}, and γ = 2500 J mol^{-1} for **1**; and ΔH_{trans} = 850 J mol^{-1}, ΔS_{trans} = 5.67 J K^{-1} mol^{-1}, and γ = 2500 J mol^{-1} for **2**. The transition fraction of **1** is 60% of that of **2**. In the calculation, ΔH_{trans} was set to 500 J mol^{-1} for **1**, which corresponds to the transition enthalpy value assuming the same fraction of transition as in **2**.

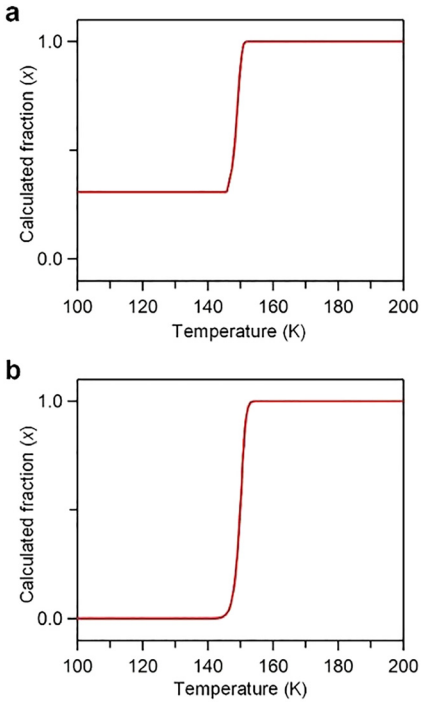

Fig. 7 Temperature dependence of the calculated fraction using the SD model, incorporating the effect of particle size distribution. The particle size distributions were assumed to follow a Gaussian distribution, with a mean size of 11.1 ± 0.2 nm for (a) **1** and 29.6 ± 0.4 nm for (b) **2** (Fig. S7).

Next, the effect of crystallite size distribution on the phase transition was considered. Assuming an average crystallite size of 11 nm for **1** and 30 nm for **2**, which possess the size distributions shown in Fig. S7, we investigated the effect of the size variation. Based on our previous findings for trititanium pentoxide,[35] where ΔH_{trans} was observed to vary approximately linearly with particle size, we used the expected ΔH_{trans} values (inset in Fig. S7) in SD model calculations (SI, S8). As shown in Fig. 7, the calculated transition fraction for **1** was approximately 60% of that for **2**, consistent with experimental observations. These results indicate that crystallite size strongly influences phase transition behavior. Specifically, phase transition **I** is progressively suppressed as the crystallite size decreases.

Conclusions

In this study, Ti_4O_7 with a controlled nanoscale crystallite size was synthesized, and the effect of crystallite size on the metal–semiconductor transition (phase transition **I**) of Ti_4O_7 was investigated. The temperature-dependent magnetic susceptibility measurements revealed that the transition fraction for

the sample with an average crystallite size of 11 nm (**1**) was approximately 60% of that for the sample with an average crystallite size of 30 nm (**2**). This suppression of the phase transition is attributed to the nanoscale effect, where a reduction in crystallite size leads to a decrease in the transition enthalpy owing to the surface energy contributions. Control over phase transitions, phenomena that critically govern the functional properties of solid materials, remains a major challenge in materials science. This study suggests that the metal–semiconductor transition in Ti_4O_7 can be effectively suppressed by reducing the crystallite size to the tens-of-nanometers scale. Based on an aqueous titanium chloride precursor, the synthesis method offers the potential to synthesize metal-substituted compounds using various metal chlorides. Therefore, the combined strategy of crystallite size control with metal substitution presents a promising route to stabilizing high-temperature metallic phases at lower temperatures.

Experimental section

Measurements: elemental analysis was performed using XRF with a RIGAKU ZSX Primus IV instrument (Energy resolution: 8.3 eV for Ti and 6.9 eV for O). The sample morphologies were measured using SEM (JEOL JSM-7500FA; spatial resolution: 1.4 nm) and TEM (JEOL JEM 2010F; spatial resolution: 0.23 nm). XRD patterns were collected using a Rigaku Ultima IV instrument with a Cu Kα light source (λ = 1.5418 Å). The 2θ step width was set at 0.02°, and the maximum deviation from the true peak position was 0.0028°. Rietveld analyses of the XRD patterns were performed using Rigaku PDXL software. The XRD patterns were calibrated using Si powder.[62] XPS spectra were recorded at room temperature using a JPS 9010 TR instrument (JEOL, Ltd, Japan; energy resolution: 1.05 eV) equipped with an ultrahigh-vacuum chamber and an Al Kα X-ray source (1486.6 eV). Terahertz time-domain spectroscopy (THz-TDS) was performed using an Advantest TAS7500 system. Magnetic measurements were performed using a Quantum Design MPMS superconducting quantum interference device (SQUID) magnetometer (magnetic moment resolution: 10^{-8} emu). The enthalpy changes associated with the phase transition were determined using a Rigaku DSC system (Thermo plus EVO2; thermal resolution: 0.1 μW), with liquid nitrogen (N_2) employed as the cooling medium.

Author contributions

T. K. conducted the sample synthesis, characterization, data analysis, and calculations, and contributed to the manuscript preparation. R. S. performed sample synthesis and characterization. T. K. also assisted with XPS measurements and their analysis. V. C. A. and M. N. performed THz conductivity measurements. S. O. contributed to data analysis. H. T. designed and supervised the study, contributed to all measurements and calculations, and wrote the manuscript. All authors participated in discussions and revision of the manuscript.

Conflicts of interest

The authors declare no competing financial interests.

Data availability

The data supporting the findings of this study are available from the corresponding author upon reasonable request.

Supplementary information (SI): crystallographic data, size distribution, TEM images, XPS spectra, THz conductivity spectrum, temperature dependence of Gibbs free energy, Gaussian distribution of the crystallite size, and relationship between Gibbs free energy, crystallite size, and transition enthalpy. See DOI: https://doi.org/10.1039/d5ma01459j.

Acknowledgements

This research was supported in part by the Japan Science and Technology FOREST Program (JPMJFR213Q), the Japan Society for the Promotion of Science Grant-in-Aid for Scientific Research (B) (22H02046), Scientific Research (A) (25H00866), Scientific Research (A) (24H00317), Transformative Research Areas (24H02232) from JSPS KAKENHI, and the JST Advanced Technologies for Carbon-Neutral (JPMJAN23A2). We are grateful to Prof. Asuka Namai for valuable technical support. We also acknowledge the support of the Cryogenic Research Center and the Center for Nano Lithography & Analysis at the University of Tokyo, which was supported by MEXT.

References

1 R. F. Bartholomew and D. R. Frankl, Electrical properties of some titanium oxides, *Phys. Rev.*, 1969, **187**, 828–833.
2 S. Lakkis, C. Schlenker, B. K. Chakraverty, R. Buder and M. Marezio, Metal-insulator transitions in Ti_4O_7 single crystals: Crystal characterization, specific heat, and electron paramagnetic resonance, *Phys. Rev. B: Solid State*, 1976, **14**, 1429–1440.
3 J. R. Smith, R. L. Clarke and F. C. Walsh, Electrodes based on Magnéli phase titanium oxides: the properties and applications of Ebonex® materials, *J. Appl. Electrochem.*, 1998, **28**, 1021–1033.
4 B. Xu, H. Y. Sohn, Y. Mohassab and Y. Lan, Structures, preparation and applications of titanium suboxides, *RSC Adv.*, 2016, **6**, 79706–79722.
5 X. Wu, H. Wang and Y. Wang, A Review: Synthesis and applications of titanium sub-oxides, *Materials*, 2023, **16**, 6874.
6 M. G. Sensoy, R. W. Carpick, D. J. Srolovitz and A. M. Rappe, Manipulating the electrical properties of conductive substoichiometric titanium oxides, *Phys. Rev. B*, 2024, **109**, 064106.
7 G. Hasegawa, T. Sato, K. Kanamori, K. Nakano and T. Yajima, Hierarchically porous monoliths based on N-Doped reduced titanium oxides and their electric and electrochemical properties, *Chem. Mater.*, 2013, **25**, 3504–3512.

8 S. Y. Huang, P. Ganesan, H. Y. Jung and B. N. Popov, Development of supported bifunctional electrocatalysts for unitized regenerative fuel cells applications, *J. Power Sources*, 2012, **198**, 23–29.
9 T. Ioroi, Z. Siroma, N. Fujiwara, S. Yamazaki and K. Yasuda, Sub-stoichiometric titanium oxide-supported platinum electrocatalyst for polymer electrolyte fuel cells, *Electrochem. Commun.*, 2005, **7**, 183–188.
10 T. Ioroi, H. Senoh, S. Yamazaki, Z. Siroma, N. Fujiwara and K. Yasuda, Stability of corrosion-resistant Magnéli-phase Ti_4O_7-supported PEFMC catalysts at high potentials, *J. Electrochem. Soc.*, 2008, **155**, B321.
11 F. C. Walsh and R. G. A. Wills, The continuing development of Magnéli phase titanium sub-oxides and Ebonex® electrodes, *Electrochim. Acta*, 2010, **55**, 6342–6351.
12 L. Zhang, J. Kim, J. Zhang, F. Nan, N. Gauquelin, G. A. Botton, P. He, R. Bashyam and S. Knights, Ti_4O_7 supported Ru@Pt core-shell catalyst for CO-tolerance in PEM in PEM fuel cell hydrogen oxidation reaction, *Appl. Energy*, 2013, **103**, 507–513.
13 X. Tao, J. Wang, Z. Ying, Q. Cai, G. Zheng, Y. Gan, H. Huang, Y. Xia, C. Liang, W. Zhang and Y. Cui, Strong sulfur binding with conducting Magnéli-phase Ti_nO_{2n-1} nanomaterials for improving lithium-sulfur batteries, *Nano Lett.*, 2014, **14**, 5288–5294.
14 Q. Pang, D. Kundu, M. Cuisinier and L. F. Nazar, Surface-enhanced redox chemistry of polysulphides on a metallic and polar host for lithium-sulfur batteries, *Nat. Commun.*, 2014, **5**, 4759.
15 L. Guo, Y. Jing and B. P. Chaplin, Development and characterization of ultrafiltration TiO_2 Magnéli phase reactive electrochemical membranes, *Environ. Sci. Technol.*, 2016, **50**, 1428–1436.
16 S. Mei, C. J. Jafta, I. Lauermann, Q. Ran, M. Kärgell, M. Ballauff and Y. Lu, Porous Ti_4O_7 particles with interconnected-pore structure as a high-efficiency polysulfide mediator for lithium-sulfur batteries, *Adv. Funct. Mater.*, 2017, **27**, 1701176.
17 K. B. Ibrahim, W. N. Su, M. C. Tsai, S. A. Chala, A. W. Kahsay, M. H. Yeh, H. M. Chen, A. D. Duma, H. Dai and B. J. Hwang, Robust and conductive Magnéli Phase Ti_4O_7 decorated on 3D-nanoflower NiRu-LDH as high-performance oxygen reduction electrocatalyst, *Nano Energy*, 2018, **47**, 309–315.
18 J. E. Won, D. H. Kwak, S. B. Han, H. S. Park, J. Y. Park, K. B. Ma, D. H. Kim and K. W. Park, PtIr/Ti_4O_7 as a bifunctional electrocatalyst for improved oxygen reduction and oxygen evolution reactions, *J. Catal.*, 2018, **358**, 287–294.
19 S. Lee, G. H. Lee, J. C. Kim and D. W. Kim, Magnéli-phase Ti_4O_7 nanosphere electrocatalyst support for carbon-free oxygen electrodes in lithium-oxygen batteries, *ACS Catal.*, 2018, **8**, 2601–2610.
20 T. Ioroi, Z. Siroma, S. Yamazaki and K. Yasuda, Electrocatalysts for PEM fuel cells, *Adv. Energy Mater.*, 2019, **9**, 1801284.
21 H. Lin, R. Xiao, R. Xie, L. Yang, C. Tang, R. Wang, J. Chen, S. Lv and Q. Huang, Defect engineering on a Ti_4O_7 electrode Ce^{3+} doping for the efficient electrooxidation of perfluorooctanesulfonate, *Environ. Sci. Technol.*, 2021, **55**, 2597–2607.
22 X. Cao, C. Wei, X. Zheng, K. Zeng, X. Chen, M. H. Rummeli, P. Strasser and R. Yang, Ru clusters anchored on Magnéli phase Ti_4O_7 nanofibers enables flexible and highly efficient Li-O_2 batteries, *Energy Storage Mater.*, 2022, **50**, 355–364.
23 W. Yang, T. Chen, H. Jia, J. Li and B. Liu, Preparation and electrochemical applications of Magnéli phase titanium suboxides: A Review, *Chem. – Eur. J.*, 2024, **30**, e202402188.
24 Z. Li, Y. Mu, Q. Zhang, H. Huang, X. Wei, L. Yang, G. Wang, T. Zhao, G. Wu and L. Zeng, Constructing highly durable reversal-tolerant anodes *via* integrating high-surface area Ti_4O_7 supported Pt and Ir@IrO_x for proton exchange membrane fuel cells, *Energy Environ. Sci.*, 2024, **17**, 1580–1591.
25 H. Tokoro, M. Yoshikiyo, K. Imoto, A. Namai, T. Nasu, K. Nakagawa, N. Ozaki, F. Hakoe, K. Tanaka, K. Chiba, R. Makiura, K. Prassides and S. Ohkoshi, External stimulation-controllable heat-storage ceramics, *Nat. Commun.*, 2015, **6**, 7037.
26 Y. Zhang, X. Li, J. Li, C. Ma, L. Guo and X. Meng, Solor-driven phase change microencapsulation with efficient Ti_4O_7 nanoconverter for latent heat storage, *Nano Energy*, 2018, **53**, 579–586.
27 M. Wang, W. Huang, Z. Shen, J. Gao, Y. Shi, T. Lu and Q. Shi, Phase evolution and formation of λ phase in Ti_3O_5 induced by magnesium doping, *J. Alloys Compd.*, 2019, **774**, 1189–1194.
28 S. Ohkoshi, H. Tokoro, K. Nakagawa, M. Yoshikiyo, F. Jia and A. Namai, Low-pressure-responsive heat storage ceramics for automobiles, *Sci. Rep.*, 2019, **9**, 13203.
29 Y. Araki, S. Ohkoshi and H. Tokoro, Synthesis of λ-Ti_3O_5 nanocrystals using a block copolymer, *Mater. Today Energy*, 2020, **18**, 100525.
30 Y. Nakamura, Y. Sakai, M. Azuma and S. Ohkoshi, Long-term heat-storage ceramics absorbing thermal energy from hot water, *Sci. Adv.*, 2020, **6**, eaaz5264.
31 S. Jütten and T. Bredow, First-principles investigation of electronic properties and phase transition of Ti_3O_5, *J. Phys. Chem. C*, 2022, **126**, 7809–7817.
32 S. Ohkoshi, F. Jia, M. Yoshikiyo, K. Imoto, H. Tokoro, K. Nakagawa, Y. Maeno, A. Namai, R. Harada, K. Hattori, K. Kojima, K. Sugiura and T. Suganuma, Pressure effect on long-term heat storage ceramics based on Mg-substituted λ-Ti_3O_5, *Mater. Adv.*, 2022, **3**, 4824–4830.
33 S. Ohkoshi, M. Yoshikiyo, J. MacDougall, Y. Ikeda and H. Tokoro, Long-term heat-storage materials based on λ-Ti_3O_5 for green transformation (GX), *Chem. Commun.*, 2023, **59**, 7875–7886.
34 S. Jütten and T. Bredow, Doping effect on the electronic structure and heat-storage properties of Ti_3O_5, *J. Phys. Chem. C*, 2023, **127**, 10445–10452.
35 T. Kubota, R. Seiki, A. Fujisawa, A. F. Fadilla, F. Jia, S. Ohkoshi and H. Tokoro, Synthesis of heat storage ceramic λ-Ti_3O_5 using titanium chloride as the starting material, *Mater. Adv.*, 2024, **5**, 3832–3837.

36 T. Otake, L. Wang, F. Jia, M. Yoshikiyo, K. Kawakami, A. Namai, H. Tokoro and S. Ohkoshi, Long–term heat–storage ceramics based on Zr-substituted λ-Ti_3O_5, *Eur. J. Inorg. Chem.*, 2024, e20240047.

37 S. Ohkoshi, Y. Tsunobuchi, T. Matsuda, K. Hashimoto, A. Namai, F. Hakoe and H. Tokoro, Synthesis of a metal oxide with a room–temperature photoreversible phase transition, *Nat. Chem.*, 2010, **2**, 539–545.

38 D. S. Ko, S. Kim, T. Y. Ahn, S. D. Kim, Y. H. Oh and Y. W. Kim, Effect of the electrode materials on the resistive switching of Ti_4O_7, *Appl. Phys. Lett.*, 2012, **101**, 053502.

39 A. Asahara, H. Watanabe, H. Tokoro, S. Ohkoshi and T. Suemoto, Ultrafast dynamics of photoinduced semiconductor-to-metal transition in the optical switching nano-oxide Ti_3O_5, *Phys. Rev. B: Condens. Matter Mater. Phys.*, 2014, **90**, 014303.

40 H. Li, T. Zhou, S. Hu, Z. Su and Y. Yan, Ti_6O_{11} nanofiber: A new material with robust switching characteristic for memories, *Chem. Eng. J.*, 2017, **312**, 328–335.

41 C. Mariette, M. Lorenc, H. Cailleau, E. Collet, L. Guérin, A. Volte, E. Trzop, R. Bertoni, X. Dong, B. Lépine, O. Hernandez, E. Janod, L. Cario, V. Ta Phauoc, S. Ohkoshi, H. Tokoro, L. Patthey, A. Babic, I. Usov, D. Ozerov, L. Sala, S. Ebner, P. Böhler, A. Keller, A. Oggenfuss, T. Zmofing, S. Redford, S. Vetter, R. Follath, P. Juranic, A. Schreiber, P. Beaud, V. Esposito, Y. Deng, G. Ingold, M. Chergui, G. F. Mancini, R. Mankowsky, C. Svetina, S. Zerdane, A. Mozzanica, A. Bosak, M. Wulff, M. Levantino, H. Lemke and M. Cammarata, Strain wave pathway to semiconductor-to-metal transition revealed by time-resolved X-ray powder diffraction, *Nat. Commun.*, 2021, **12**, 1239.

42 Y. Hu, H. Mba, M. Picher, H. Tokoro, S. Ohkoshi, C. Mariette, R. Mandal, M. Alsahoor, P. Rabiller, M. Lorenc and F. Banhart, Phase transformations of individual Ti_3O_5 nanocrystals studied by In Situ electron microscopy, *J. Phys. Chem. C*, 2024, **128**, 13991–13997.

43 C. Schlenker and M. Marezio, The order–disorder transition of Ti^{3+}–Ti^{3+} pairs in Ti_4O_7 and $(Ti_{1-x}V_x)_4O_7$, *Philos. Mag. B*, 1980, **42**, 453–472.

44 C. Schlenker, S. Lakkis, J. M. D. Coey and M. Marezio, Heat capacity and metal-insulator transitions in Ti_4O_7 single crystals, *Phys. Rev. Lett.*, 1974, **32**, 1318–1321.

45 M. Marezio, D. B. McWhan, P. D. Dernier and J. P. Remeika, Structural aspects of the metal-insulator transitions in Ti_4O_7, *J. Solid State Chem.*, 1973, **6**, 213–221.

46 M. Marezio, D. B. McWhan, P. D. Dernier and J. P. Remeika, Charge localization at metal-insulator transitions in Ti_4O_7 and V_4O_7, *Phys. Rev. Lett.*, 1972, **28**, 1390–1393.

47 M. Marezio, P. D. Dernier, D. B. McWhan and J. P. Remeika, X-ray diffraction studies of the metal-insulator transitions in Ti_4O_7, V_4O_7, and VO_2, *Mat. Res. Bull.*, 1970, **5**, 1015–1024.

48 R. Macnas, J. Ranninger and S. Robaszkiewicz, Superconductivity in narrow-band systems with local nonretarded attractive interactions, *Rev. Mod. Phys.*, 1990, **62**, 113–171.

49 L. J. De Jongh, A Comparative Study of (Bi)Polaronic (Super)-Conductivity in High- and Low-T_c Superconducting Oxides, *Physica C*, 1988, **152**, 171–216.

50 B. K. Chakraverty, Possibility of insulator to superconductor phase transition, *J. Phys., Lett.*, 1979, **40**, 99–100.

51 H. Ueda, K. Kitazawa, H. Takagi and T. Matsumoto, Strong Carrier Concentration Dependence of Pressure Effect on Bipolaronic Transitions in Magnéli Phase in Ti_nO_{2n-1} (n = 4, 5, 6), *J. Phys. Soc. Jpn.*, 2002, **71**, 1506–1510.

52 T. Tonogai, H. Takagi, C. Murayama and N. Mori, Metal-insulator transitions in Ti_4O_7: Pressure-induced melting of the electron pairs, *Rev. High Pressure Sci. Technol.*, 1998, **7**, 453–455.

53 J. L. Hodeau and M. Marezio, Structural aspects of the metal-insulator transitions in $(Ti_{0.9975}V_{0.0025})_4O_7$, *J. Solid State Chem.*, 1979, **29**, 47–62.

54 C. Schlenker, S. Ahmed, R. Buder and M. Gourmala, Metal-insulator transitions and phase diagram of $(Ti_{1-x}V_x)_4O_7$: electrical, calorimetric, magnetic and EPR studies, *J. Phys. C: Solid State Phys.*, 1979, **12**, 3503–3521.

55 S. Ahmed, C. Schlenker and R. Buder, Metal-insulator Transitions in $(Ti_{1-x}V_x)_4O_7$, *J. Magn. Mag. Mater.*, 1978, **7**, 338–340.

56 C. Schlenker, S. Lakkis, S. Ahmed, J. L. Hodeau and M. Marezio, Metal-insulator transitions in $(Ti_{1-x}V_x)_4O_7$, *J. Phys. C: Solid State Phys*, 1977, **10**, L151–L156.

57 K. Yoshimatsu, O. Sakata and A. Ohmoto, Superconductivity in Ti_4O_7 and γ-Ti_3O_5 films, *Sci. Rep.*, 2017, **7**, 12544.

58 H. Tokoro, Y. Araki, I. Nagata, T. Kondo, K. Imoto and S. Ohkoshi, Synthesis of nanosize tetratitanium heptoxide and its anomalous phase transition, *Mater. Res. Lett.*, 2020, **8**, 261–267.

59 D. Kundu, R. Black, E. J. Berg and L. F. Nazar, A highly active nanostructured metallic oxide cathode for aprotic Li–O_2 batteries, *Energy Environ. Sci.*, 2015, **8**, 1292–1298.

60 M. Taguchi, A. Chainani, M. Matsunami, R. Eguchi, Y. Tanaka, K. Tamasaku, Y. Nishino, T. Ishikawa, S. Tsuda, S. Watanabe, C. T. Chen, Y. Senda, H. Ohashi, K. Fujiwara, Y. Nakamura, H. Takagi and S. Shin, Anomalous state sandwiched between fermi liquid and charge ordered mott-insulating phase of Ti_4O_7, *Phys. Rev. Lett.*, 2010, **104**, 106401.

61 C. P. Slichter and H. G. Drickamer, Pressure-induced electronic changes in compounds of iron, *J. Chem. Phys.*, 1972, **56**, 2142–2160.

62 Y. S. Touloukian, R. K. Kirby, R. E. Taylor and T. Y. R. Lee, *Thermal expansion: nonmetallic solids*, IFI/Plenum, New York, 1977.